STEREOSCOPIC FLAT PANEL DISPLAY

Brian K. Jones* & James C. Kirsch
U.S. Army AMRDEC
AMSRD-AMR-WS-PL
Redstone Arsenal, Alabama 35898

John L. Johnson
HQ, USAEUR & 7th Army
Office of the Science Advisor
Unit 29351, APO AE 09014

ABSTRACT

Stereo imagery has been a goal in optics research since the invention of the stereoscope in 1834. While the market has been inundated with displays of various types, sizes, and formats, no general purpose, easy to use, inexpensive method for the display of imagery in stereo has been developed. The benefits of stereo vision are numerous and quickly become apparent when attempting to perform simple tasks without the aid of stereo cues. The proliferation of remotely operated vehicles and indirect view applications has resulted in an increased need to see the operational environment in stereo.

Numerous approaches to the display of stereo imagery have been demonstrated. Stereoscopic displays typically require the user to wear special headgear. Autostereoscopic displays, so named because they do not require the headgear, typically have tight limitations on the position of the viewer's head. Previous papers have described the theoretical underpinnings for new type of stereoscopic displayed based on dual liquid crystal displays. The new display provides a stereo view without temporal or spatial multiplexing. This paper will present the results from experiments to characterize the display components and the resulting changes in the encoding algorithm.

Keywords: Stereoscopic display, LCD, 3D, polarization encoding, flat panel

1. INTRODUCTION

The use of remotely operated vehicles has been rapidly increasing in recent years. Remotely operated, in this case, also refers to situations where an operator rides in the vehicle but is not permitted a direct view of the outside world. There are several scenarios where this may be the case, including situations where the operator's eyes must be protected or where night vision is required. These cases usually require the operator to control the vehicle while viewing the outside world on a monitor or flat panel display. The disadvantage of limiting the viewer to a flat panel display is the loss of many of the depth cues needed to avoid obstacles. Several serious accidents have occurred where the operator misjudged the distance to (or depth of) a ditch in the field of view. One solution to this problem is to provide the operator with stereoscopic vision that restores depth perception. The operating conditions for many applications require the stereo display to be compact and rugged while still providing the necessary depth cues to the driver. Such a system would also be useful for remotely piloted vehicles, remotely operated spacecraft, planetary rovers, deep sea applications, or any other environment dangerous to human operators.

The Weapons Sciences Directorate of the U.S. Army Aviation & Missile Research, Development, and Engineering Center has recently developed a stereoscopic display based on dual liquid crystal panels such as those found in laptop computers. The basic idea is a polarization encoded display but in a compact package suitable for use in fielded environment. The packaged display is no larger than standard flat panel displays already in use and only slight thicker. The panels themselves are relatively cheap so the main cost is in providing the stereo (left & right) views of the world to the panels. The advantages of this display approach over other stereoscopic displays are the full frame rate (no temporal multiplexing), full spatial resolution (no spatial multiplexing), and the compact design (no projection optics). The user is required to wear inexpensive polarized glasses. The display can also be used as a regular flat panel display when viewing non-stereoscopic imagery or data.

Remotely operated vehicles do not represent the only potential application for 3D vision. Human operators find it easier to detect regions of interest in 3D imagery than in 2D imagery. Applications in this area abound including, but not limited to, medical diagnostic imagery, reconnaissance imagery, and, perhaps, homeland security. The entertainment industry has experimented with different types of 3D imagery for years and appears

Report Documentation Page

Form Approved
OMB No. 0704-0188

1. REPORT DATE	2. REPORT TYPE	3. DATES COVERED
00 DEC 2004	**N/A**	**-**

4. TITLE AND SUBTITLE	5a. CONTRACT NUMBER
Stereoscopic Flat Panel Display	5b. GRANT NUMBER
	5c. PROGRAM ELEMENT NUMBER
6. AUTHOR(S)	5d. PROJECT NUMBER
	5e. TASK NUMBER
	5f. WORK UNIT NUMBER
7. PERFORMING ORGANIZATION NAME(S) AND ADDRESS(ES) **U.S. Army AMRDEC AMSRD-AMR-WS-PL Redstone Arsenal, Alabama 35898; HQ, USAEUR & 7th Army Office of the Science Advisor Unit 29351, APO AE 09014**	8. PERFORMING ORGANIZATION REPORT NUMBER
9. SPONSORING/MONITORING AGENCY NAME(S) AND ADDRESS(ES)	10. SPONSOR/MONITOR'S ACRONYM(S)
	11. SPONSOR/MONITOR'S REPORT NUMBER(S)

12. DISTRIBUTION/AVAILABILITY STATEMENT
Approved for public release, distribution unlimited

13. SUPPLEMENTARY NOTES
See also ADM001736, Proceedings for the Army Science Conference (24th) Held on 29 November - 2 December 2005 in Orlando, Florida.

14. ABSTRACT

15. SUBJECT TERMS

16. SECURITY CLASSIFICATION OF:			17. LIMITATION OF ABSTRACT	18. NUMBER OF PAGES	19a. NAME OF RESPONSIBLE PERSON
a. REPORT	b. ABSTRACT	c. THIS PAGE			
unclassified	**unclassified**	**unclassified**	**UU**	**8**	

determined to provide a virtual 3D gaming experience in future generations of video games. The nature of the invention described here makes it an ideal candidate for incorporation into laptop computers for high-end applications.

2. DUAL PANEL 3D DISPLAY

Polarization has been used in the past as a tool for separating left and right stereo pairs. Liquid crystal displays (LCDs) are also commonly used for stereoscopic displays. The techniques used previously, however, suffered from complicated optics, reduced resolution, reduced frame rate, bulky packaging, and other drawbacks that made them somewhat undesirable (Lane, 1982; Chen et al., 1997). The approach described here attempts to address some of these issues. Two LCDs were stacked together to form a compact panel capable of displaying stereo images without loss of resolution or frame rate. The approach does require the user to wear polarization glasses, similar to ones used in 3D movies.

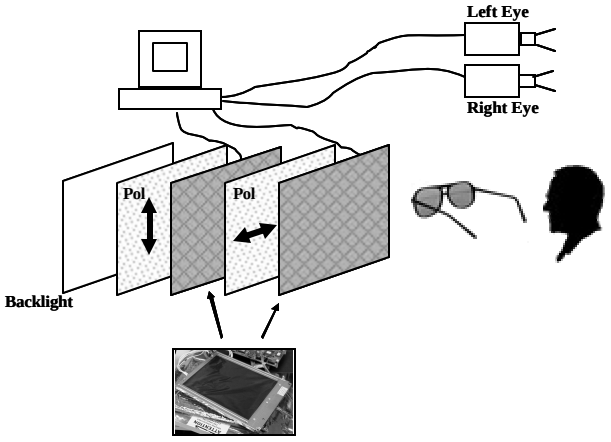

Fig. 1. Block diagram of stereoscopic display.

The proposed architecture is shown in Figure 1. The stereoscopic display was constructed from two Sharp LQ104V1DC31 10.4" LCD panels. A standard backlight provides the necessary illumination for the display. The first panel, closest to the backlight, retains both the input and output polarizers. In essence, this is the standard liquid crystal display. The presence of the polarizers means that irradiance images are visible on the display and, in fact, this display is used to control the total irradiance in the system. A second liquid crystal panel is added to the stack for the stereoscopic display. This panel is identical to the first panel with the exception that both polarizers have been removed. The second panel serves as an array of variable ½ wave retarders that control the polarization orientation of the output light. This panel is used to encode the left and right image data which is then decoded by polarized glasses on the observer.

Mathematically, the process is described as follows:

$$I_T = \frac{I_L(x,y) + I_R(x,y)}{2} \quad (1)$$

where $I_L(x,y)$ is the image irradiance distribution captured by the 'Left Eye' camera, $I_R(x,y)$ is the image irradiance distribution captured by the 'Right Eye' camera, and $I_T(x,y)$ is the total irradiance in the resulting integrated image. The first panel, with both front and back polarizers, is used to encode this intensity image.

Now that the total intensity for the stereo pairs has been encoded, superposition will be used to divide that intensity between the left and right eyes of the observer. Consider the polarization state of the light entering the second LCD panel. All of the light exiting from the first (irradiance) panel and polarizer set has the same polarization as determined by the output polarizer. The second panel has no polarizers but each pixel of the liquid crystal panel rotates the polarization of the incident light by an amount determined by the state of that pixel. The polarization state upon leaving the first panel is illustrated in Figure 2(a). The polarization state after passing through the second panel at an arbitrary pixel is shown in Figure 2(b). The amplitude of the light leaving the first panel determines the length of the electric field vector (E_T). The orientation of that vector is determined by the amount of rotation imparted by the second panel. Superposition can be used to write the orientation of that vector in terms of orthogonal polarizations referred to as $E_L(x,y)$ and $E_R(x,y)$. The polarizing glasses worn by the observer will now preferentially pass these two

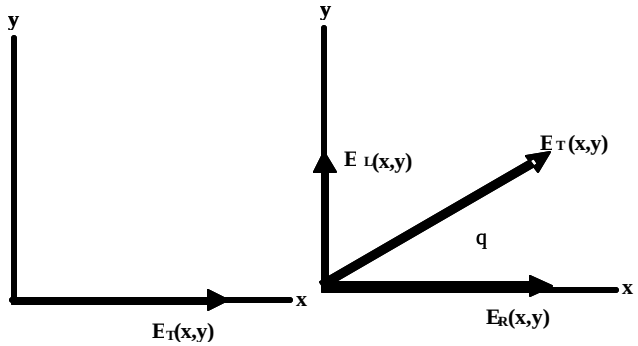

(a) (b)

Fig. 2. (a) Polarization orientation of light leaving irradiance panel and polarizer. (b) Polarization orientation of light leaving an arbitrary pixel of the polarization panel.

components to the appropriate eye. Therefore, how the light is divided between the two eyes is determined by the orientation of the electric field vector (E_T) leaving the second panel. Changing the orientation of the electric field vector changes the amount of light reaching each eye. In this manner, the light leaving the second panel can be directed to the appropriate eye for the left and right stereo pairs.

From Malus's Law, the irradiance of the light passing through an analyzer can be written as:

$$I_R(x,y) = I_T(x,y)\cos^2 q = \left[I_L(x,y) + I_R(x,y)\right]\cos^2 q \qquad (2)$$

$$\cos^2 q = I_R(x,y) / \left[I_L(x,y) + I_R(x,y)\right] \qquad (3)$$

where I_L is the irradiance in the left image, I_R is the irradiance in the right image, and θ is the polarization angle from Figure 2(b) This illustration assumes the transmission axis of the analyzers in front of the left and right eyes are oriented along the x-axis and y-axis, respectively.

The images in Figure 3 illustrate the process of encoding the stereo images. Images from the left and right cameras are combined according to Eq. 1 to form the irradiance image. The resulting image shows the disparity between the left and right views. The images are combined according to Eq. 3 to form the polarization image. Comparing the image with the diagram in Figure 2(b), yields confidence that the algorithm is working as expected. Bright areas of the image correspond to most of the light going to one eye, while darker areas correspond to most of the light directed to the other eye. Regions of medium gray are areas where the light is approximately divided evenly between the two eyes. As an example, compare the position of the chair arm in the top and bottom images. It is easy to see that the chair arm in the top image appears farther to the left than the arm in the bottom image. In the composite polarization image, the arm appears twice - darker on the left and brighter on the right. This corresponds to directing the light from the arm to different eyes. The resulting disparity gives rise to the perception of depth.

(2)

3. COMPONENT EVALUATION

The panel chosen for this initial work, the Sharp LQ104V1DC31, is shown in Fig. 4. This is a 10.4" diagonal panel with 640x480x3 pixels, where the pixels are arranged in an RGB fashion to produce a color image. The initial experiments were performed with grayscale images; however, the technique can easily be applied to produce a color image. The panels can be individually driven with either a standard NTSC video signal or a

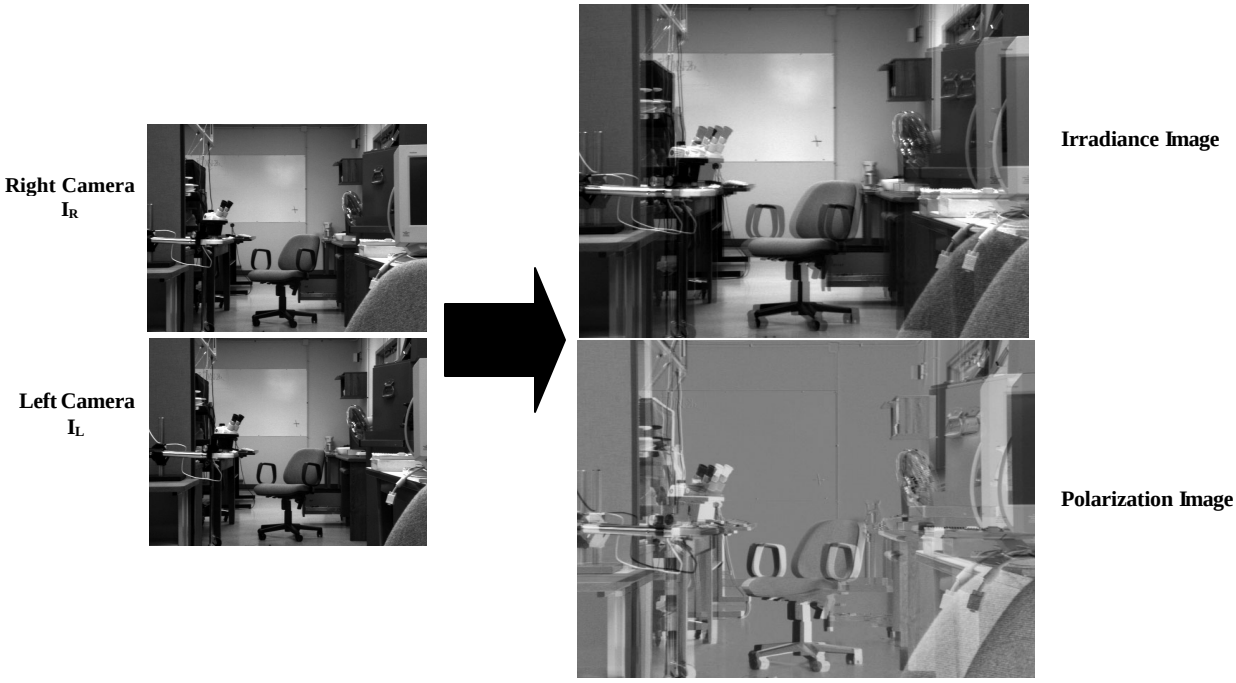

Fig. 3. Left and right eye views are combined to form the irradiance and polarization images. White areas in the polarization image correspond to all light going to one eye while dark areas correspond to all light going to the other.

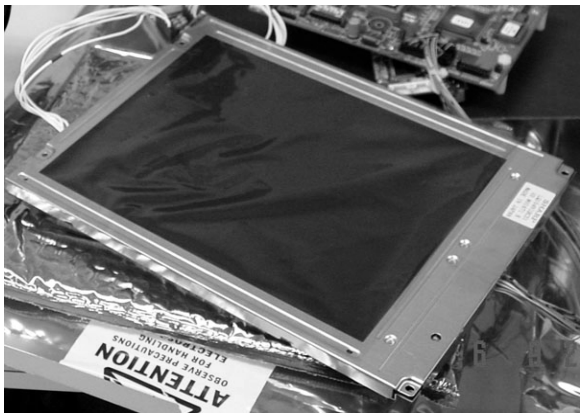

Fig. 4. Photograph of the Sharp LQ104V1DC31 liquid crystal panel.

digital 640x480 computer video signal through a Digital View ACL-1024 video controller. The performance of the individual panels will determine the overall performance of the 3D display as well as dictate how the algorithm must be modified to maximize performance.

The algorithm described above makes two key assumptions about the modulation characteristics of the liquid crystal panels. First, it assumes that the panels are capable of providing a variable 0 to 90 degree change in the orientation of the polarization vector. Second, it assumes that the modulation curve is linear. Neither of these assumptions is likely to be correct in an off-the-shelf device. Initial attempts to generate the stereoscopic images with the Sharp panels and the algorithm discussed were sufficient to prove the concept, but also indicated that a better understanding of the modulation characteristics was required. The stereoscopic images were discernible however, significant ghosting was also present. Ghosting refers to seeing left eye image data with the right eye and vice versa.

A Stokes vector imaging polarimeter was constructed to analyze the modulation characteristics of the liquid crystal panels. A diagram of the polarimeter is shown in Fig. 5. This particular configuration is frequently referred to as a rotating waveplate polarimeter. The polarimeter consists of a rotating ¼ waveplate, a fixed linear polarizer, and an imaging detector. The rotating waveplate is placed at an intermediate image plane to minimize wedge effects. The calibration procedure and methods for analyzing the data to determine unknown polarization states are discussed in the literature (Chenault, 1992).

The Stokes vector polarimeter is designed to determine the polarization state of the unknown input light. In this particular case, the unknown polarization state is a result of the liquid crystal panel. Linearly polarized light at a known orientation is incident on the liquid crystal panel with no polarizers. Relay lenses between the liquid crystal panel and the rotating waveplate are not shown. The Stokes vector of the light after passing through the panel was determined as a function of pixel grayscale as well as brightness and contrast. Lenses in the system magnify the image of the liquid crystal panel such that individual pixels are visible

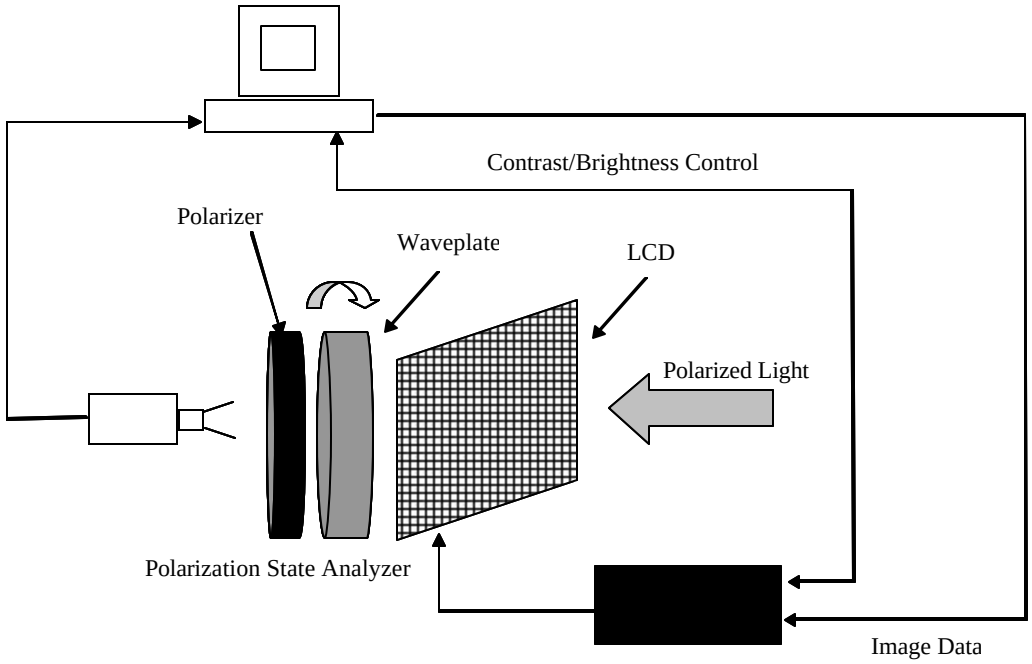

Fig. 5. Diagram of the Stokes vector polarimeter used to characterize the liquid crystal panels.

on the detector. It is important to note that the color filter in the panel will affect the results. At a minimum, the retardance of the waveplate is a function of wavelength. The individual pixels were imaged onto the detector so that data could be collected for red, green, and blue pixels in order to account for wavelength in the characterization. The input polarized light was provided by a Labsphere USS-600 uniform illumination source. The uniform source provides white light with a uniform luminance over a 2" diameter aperture. The light is then polarized by a Melles Griot dichroic sheet polarizer like the 03 FPG 007.

The first step in determining the polarization modulation characteristics of the LCD was to determine the output polarization state from the intensity panel. The intensity panel was placed in the polarimeter and the detector captured sixteen intensity images as the waveplate was rotated through 360 degrees. An analysis of the data was performed to determine the Stokes vector for the light leaving the intensity panel. This polarization state was used as the starting point for calibrating the polarization (top) panel of the stereoscopic display.

The polarization panel was placed into the polarimeter with the input polarization state aligned with the output state from the intensity panel. The Stokes vector of the light leaving the polarization panel as a function of input pixel level was determined for a variety of brightness and contrast settings on the LCD. Several things were immediately apparent from this data. First, the achievable polarization rotation was approximately 70 degrees rather than the desired 90 degrees. Second, the circular polarization component of the light leaving the panel increased significantly with pixel value. Both of these conditions would lead to significant noise in the 3D image using the theoretical equations described above. Noise, in this case, is defined as unwanted light reaching the eye making it difficult to achieve an 'off' state in a particular eye.

The data collected using the manufacturer's original polarizer settings is shown here. Figure 6 is a plot of the polarization ellipse as a function of grayscale. The light leaving the panel for the lower grayscale values is relatively linear. As the pixel value increases, the light becomes more elliptical and then begins to return to a linear state. Even at a grayscale value of 255 however, the light is still fairly elliptical. It is also evident that the orientation of the polarization vector does not rotate the full 90 degrees as expected. Figure 7 is a plot of the irradiance at each eye as a function of grayscale. The graph was generated by multiplying the Stokes vector at each pixel grayscale by the Mueller matrix of a polarizer at the left and right eye orientation. The contrast between the left and right eye at a grayscale of 0 is very high. The contrast at the other end of the grayscale range is much lower. The net result is that one eye will see a very high contrast image while the other eye will lower contrast and significant ghosting. The ideal result would be for the contrast ratio to be very high and balanced on both ends of the curve.

The plots in Figure 6 and Figure 7 led to two conclusions. First, with less than a 90 degree change in the orientation of the polarization vector, orthogonal polarizers on the eyes are not the optimal choice. Contrast is primarily of function of how dark the "black" or "off" state is in the image. It is readily apparent that crossed polarizers were chosen by the manufacturer because the most linear state, and hence the darkest "off", occurs when the maximum voltage is applied to the panel. For the stereoscopic display, good "off" states are required on both ends of the grayscale curve. The optimal orientation for the eye polarizers is, then, orthogonal to the major axis of the polarization ellipse for the 0 and 255 graylevels. One eye polarizer is chosen to be orthogonal to the major axis of the ellipse at graylevel 0 and the other eye polarizer chosen to be orthogonal to the major axis of the ellipse at graylevel 255.

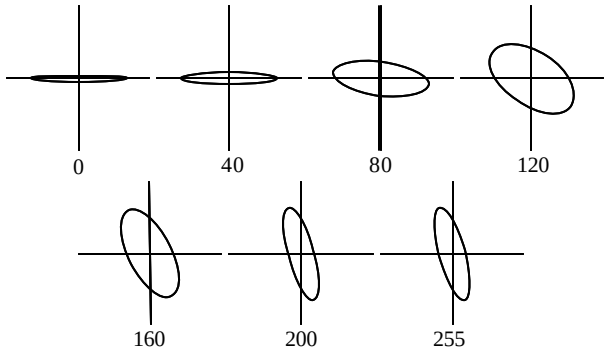

Fig. 6. Polarization ellipses with manufacturer's original polarizer orientations.

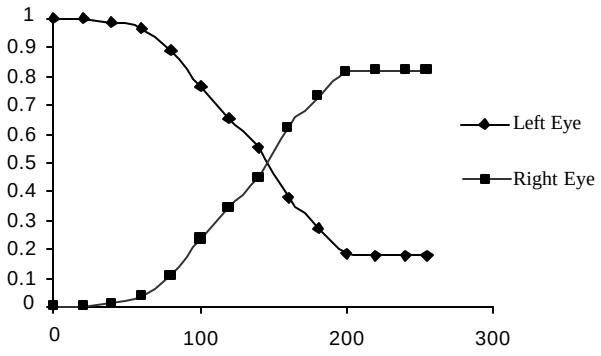

Fig. 7. Relative irradiance reach the left and right eyes as a function of pixel value.

The second conclusion was that the amount of ellipticity in the polarization vector needed to be minimized for best contrast. It was theorized that the original manufacturer's polarizer orientation was not aligned with the liquid crystal director. The Stokes vector data was collected for a variety of input polarizer orientations. Figure 8 is a plot of the polarization ellipses for the optimal input polarization orientation. The ellipticity of the polarization has been minimized, particularly at the upper end of the grayscale range. The plot in Figure 9 is the relative irradiance reaching each eye for this input polarization setting and with the optimized eye polarizer settings. The contrast is high on both ends of the grayscale.

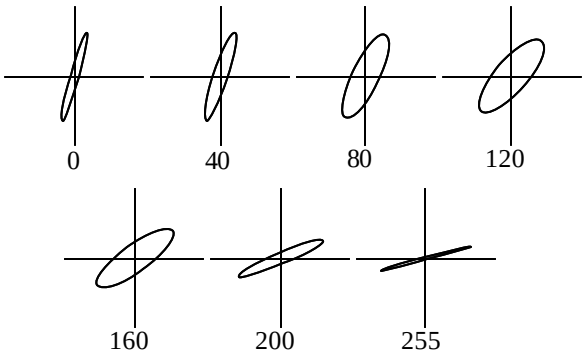

Fig. 8. Polarization ellipses for the optimized input polarization orientation.

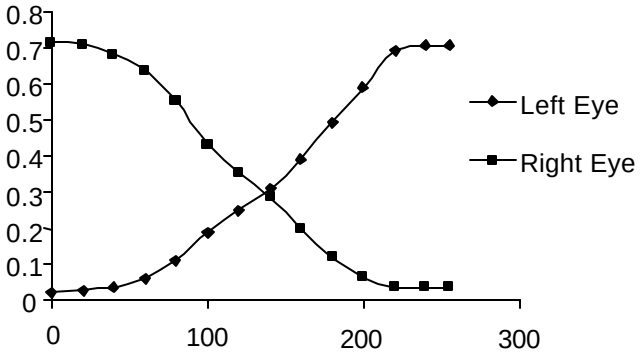

Fig. 9. Relative intensity reaching left and right eyes as a function of pixel value.

The effects of brightness and contrast were also studied. Referring to Figure 9, changes in the brightness settings cause the graph to slide left and right along the x-axis. Brightness acts as a bias that effectively sets were the pixels begin to "switch on". Contrast changes the slope of the line. Brightness and contrast settings have been optimized in Figure 9 to minimize the flat regions at the top and bottom of the curve.

4. ALGORITHM MODIFICATIONS

The curve in Figure 9 is quite clearly not the ideal curve envisioned by the original algorithm. The nonlinearities in the curve can easily be taken into account by using the curve to generate look-up tables (LUTs) for the polarization panel. The curve shown in Figure 9 is for the green pixels. Similar, but different, curves were also generated for the red and blue pixels. All of the curves have the same general shape but there are differences in slope. LUTs were generated for all three color planes (red, green, and blue). The irradiance panel curve was measured by simply inserting a power meter after the panel and measuring the relative irradiance as a function of grayscale. This curve is also used to generate a LUT for the irradiance panel.

One more factor related to the less than ideal modulation characteristics of the panels must be taken into account. The most demanding situation, in terms of available light, occurs when both the left and right images have a fully on (pixel value = 255, normalized to 1.0) pixel. The same amount of light needs to reach both the left and right eyes, which occur at the crossing point in Figure 9. The relative intensity reaching both eyes at that point, however, is only 29% of the total light available according to the plot.

Now consider the case where the left image pixel value is 255 (normalized to 1.0) and the right image pixel value is 0. From Eq. 1, the relative irradiance value would be 0.5. From Figure 9, the polarization panel relative irradiance value would be 0.71. The relative irradiance reaching the left eye is then 0.5*0.71 = 0.36. Now, in both cases, the left image value is the same and the same amount of light should reach the left eye from both pixels. The analysis shows, however, that more light is reaching the left eye when only the left image pixel is on (0.36) than when both the left and right pixels are on (0.29). The irradiance panel value must be modified so that a 255 in the left image yields the same amount of light in the left eye irrespective of the right image pixel value. The same holds true when considering the right eye.

The polarization panel is correctly dividing the light between the left and right eyes. The low transmission values result from the fact that the polarizer on each eye is oriented to provide the best "off" or black state rather than the maximum transmission. If a full 90 degree rotation was present in the panel, most of the problem would disappear. The low transmission value is unavoidable given the less than 90 degree twist. A scaling factor must

therefore be applied when determining the appropriate irradiance panel setting.

The total transmitted light reaching both eyes in the ideal case is given by:

$$I_{ideal} = \frac{I_L + I_R}{2*255} \quad (4)$$

where I_{ideal} is the total light reaching the eyes scaled from 0 to 1. The actual light reaching the two eyes (neglecting, for the moment, the nonlinearity in the irradiance panel) is given by:

$$I_{actual} = \frac{I_L + I_R}{2*255} * (L + R) \quad (5)$$

where I_{actual} is the actual total irradiance reaching both eyes, and L and R are the left and right eye transmission values from Figure 9. The second term in this equation takes into account the lower than ideal transmission values in the polarization panel/polarized glasses combination. The changing ellipticity in the polarization from the panel, as well as the non-orthogonal polarizers on the eyes, means that the quantity $L+R$ is no longer a constant. The input irradiance must be scaled to account for these factors. The maximum value of the actual total irradiance reaching both eyes can be no greater than the worst case (both pixels are 255) described above. The scaling factor is, therefore:

$$ScaleFactor = \frac{2 * T_{cross}}{(L + R)} \quad (6)$$

where T_{cross} is the transmission at the crossing point in Figure 9. The procedure, then, is to calculate the irradiance value using Eq. 1 and then scale it using Eq. 6.

5. STEREOSCOPIC DISPLAY

A photograph of the stereoscopic display is shown in Figure 10. The two panels have been sandwiched together with the polarizers on the irradiance panel aligned in the optimal configuration determined above. The algorithm has been encoded in look-up-tables to improve the performance of the software. Real time (30 Hz) frame rates with stereo cameras providing the input imagery was achieved used the look-up-table approach.

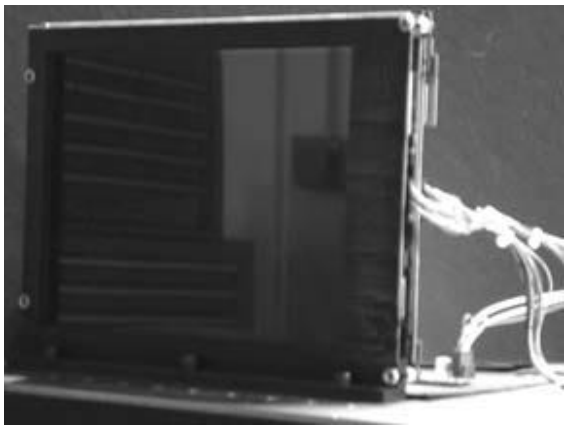

Fig. 10. Photograph of the assembled dual flat panel display.

A sample stereo pair is shown in Figure 11. The images are printed with the left image on right and the right image on the left. This is sometime referred to as the cross-eye arrangement. Viewers can see the stereo effect by allowing their eyes to cross in front of the page. The resulting virtual image that appears between the two real images should have depth. The images in Figure 11 were processed according to the algorithm described above and sent to the appropriate panels of the display. The images shown in Figure 12 were taken by viewing the stereoscopic display through the appropriate left eye

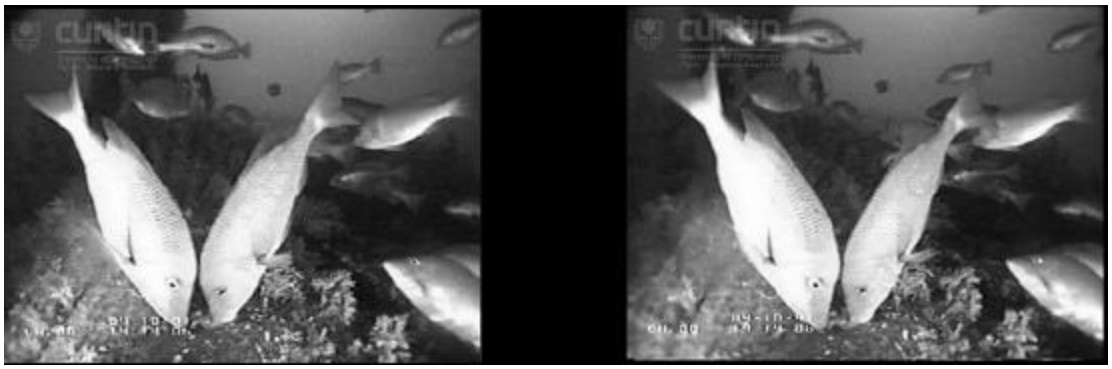

Fig. 11. Original stereo pairs in cross-eye arrangement. Images courtesy of Andrew Woods, The Centre for Marine Science & Technology at Curtin University.

Fig. 12. Photograph of fish as displayed on LCD stack and seen through the left and right eye polarizers. The left eye image is on the right so that tthe stereo effect can be viewed using the cross-eye technique.

and right eye polarizers. The images are again printed in the cross-eye format to allow the reader to see that the depth information has been retained.

The images in Figure 12 have a discernible fringe pattern across them. The fringe pattern is a result of crosstalk between pixels in the stacked arrangement. The separation between the two panels allows light from a pixel in the bottom panel to pass through an adjacent pixel in the top panel. The effect is magnified by the color filters on the panels in the sense that light passing through a blue pixel in the bottom panel might pass through an adjacent green or red pixel in the top panel.

CONCLUSION

The dual LCD flat panel display concept presented here has been validated with a working prototype. The results from the characterizations described have led to a greatly improved stereo display over the original algorithm. Procedures for determining the optimal polarizer settings for the polarization panel and the glasses as well as the required algorithm modifications have been discussed. The display offers the advantages of full resolution and full frame rate while still maintaining a rugged and compact design.

The prototype display has been demonstrated with infrared cameras to potential users as shown in Figure 13. The resulting stereo image has received considerable positive feedback and continued invitations to more demonstrations. Current efforts are focused on eliminating the fringing evident in Figure 12 and on developing dedicated drive electronics to eliminate the computer currently used for the algorithm.

Fig. 13. Display integrated with infrared cameras for demonstrations to soldiers.

REFERENCES

Lane, B., 1982: “Stereoscopic Displays,” in *Processing and Display of Three-Dimensional Data*, J.J. Pearson, ed., Proc. of the SPIE 367, 22-23.

Chen, J., Kim, K.H., Kim, N.D., Souk, J., Bos, P.J. and and Shin, S.T., 1997: “Simple Multimode Stereoscopic Liquid Crystal Display”, *Japanese Journal of Applied Physics*, **36**, 1685-1688 .

Chenault, D. B., 1992: *Infrared Spectropolarimetry*, 21-30, University of Alabama in Huntsville.